Nanoscale Res Lett (2009) 4:865–872
DOI 10.1007/s11671-009-9337-3

NANO EXPRESS

# Use of Ionic Liquid in Fabrication, Characterization, and Processing of Anodic Porous Alumina

**Marco Salerno · Niranjan Patra · Roberto Cingolani**

Received: 19 February 2009 / Accepted: 24 April 2009 / Published online: 8 May 2009


**Abstract** Two different ionic liquids have been tested in the electrochemical fabrication of anodic porous alumina in an aqueous solution of oxalic acid. It was found that during galvanostatic anodization of the aluminum at a current density of 200 mA/cm$^2$, addition of 0.5% relative volume concentration of 1-butyl-3-methylimidazolium tetrafluoborate resulted in a three-fold increase of the growth rate, as compared to the bare acidic solution with the same acid concentration. This ionic liquid was also used successfully for an assessment of the wettability of the outer surface of the alumina, by means of liquid contact angle measurements. The results have been discussed and interpreted with the aid of atomic force microscopy. The observed wetting property allowed to use the ionic liquid for protection of the pores during a test removal of the oxide barrier layer.

**Keywords** Porous alumina · Anodization · Galvanostatic · Ionic liquids · Wettability · Roughness

## Introduction

Anodic porous alumina (APA [1–4]), also called porous anodic alumina (PAA) [5–9]), anodic aluminum oxide (AAO [10, 11]), or alumite [12, 13], is a form of $Al_2O_3$, which is deposited onto an aluminum (Al) foil working as the positively biased pole of an electrolytic cell [14–16]. Whereas in basic or neutral electrolytes (ELs) a compact alumina layer is grown, called "barrier" layer, in acidic ELs that can dissolve the oxide a porous alumina layer is grown, on top of a thin (10–100 nm [17]) barrier-type layer. Depending on the applications, pore ordering in APA can be necessary either on both sides such as for photonic crystals made by using APA as a lithographic mask [18], or only on one side such as for in situ photonic crystals made by incorporating materials on one APA surface [19–21], or on none of the two sides such as for filtering membranes [22–24], biosensor electrodes with enhanced surface area [4], and templates for the growth of separated metal nanowires [13, 25, 26], or supported oxide or polymer nanotubes [27, 28]. However, for several applications, it is desirable that the APA thickness $h$ is comparatively high, $h \geq 100$ μm. This can give the film the required robustness for use as either a standalone membrane in case of, e.g., battery separator [23] or lithographic etching mask [18, 29], or the required high aspect ratio (a.r. $= h/d$, where $d$ is the pore diameter) when using the layer as a template for, e.g., nanowire electrodeposition (where a.r. $\geq$ 1,000 can be required [21, 30]). However, the film growth rate $v_g$ reported so far for conventional mild anodization (MA) of Al has been in the order of 0.03–0.1 μm/min [31], which makes the growth of thick APA quite time consuming. This slow growth hinders the advantage of the relatively cheap setup for the fabrication of APA, discouraging its use for both the development of prototype structures in the research academy, and for possible industrial fabrication processes. The current interest in speeding up the APA growth has recently found a viable way in the application of a single-step process combining MA with industrial hard anodization (HA) conditions [31], made possible by the protecting oxide layer grown during the preliminary MA phase.

Another possible route for fast APA fabrication could be the identification of proper additives, which can

M. Salerno (✉) · N. Patra · R. Cingolani
Nanobiotechnology Department, The Italian Institute of Technology, via Morego 30, Genova 16163, Italy
e-mail: marco.salerno@iit.it

conveniently change the environmental conditions for anodization. Ionic liquids (ILs) are a class of solvents that have recently attracted a renewed interest as chemical additives in a number of reactions [32, 33]. To our knowledge, the only use of APA and IL system has been so far as an additive in the fabrication of cobalt nanowires inside an APA template [9]. In this work, we report on the use of ILs in the fabrication and characterization of APA, starting from a well-known APA fabrication EL such as oxalic acid. The idea behind using IL additives in this system is that the convective flow of the IL component species can facilitate the displacement of the EL ions useful for anodization, and avoid formation of strong temperature gradients between the anode and the beaker walls, which are in direct contact with the refrigerating bath.

## Materials and Methods

### Sample Fabrication

We used 0.25-mm thick foils of polycrystalline Al (Goodfellows, 99.999% purity). The foils were cut with scissors into rectangular pieces of single face area $S \sim 15 \times 3$ mm$^2$, and flattened back to roughly planar surface, after scissors curling, by pressing each of them between two new glass slides.

Degreasing was performed by hand brushing (>10 s) with acetone-wet lens paper, 3 min sonicating in warm (60 °C) acetone, rinsing in de-ionized (DI) water, sonicating another 3 min in warm (60 °C) ethanol, and thoroughly washing (>30 s) in running DI water.

After degreasing, an electropolishing (EP) step was performed on the Al foil, which was partly dipped in a 250-mL beaker filled up to 200 mL with a 1:5 v/v $HClO_4$:-$C_2H_5OH$ mixture, and kept inside a refrigerating bath set at $T_{bath}$ =+7 °C. The cathode was a Pt plate, also partly dipped in the EL, kept at a gap distance of $g \sim 11$ mm from the Al anode. The process was run for 7 min without stirring, at constant current $i_{EP}$.

In our setup, both sides of the dipped Al foil come into contact with the EL, the anodic contact being provided from the top, outside the EL. The dipped single face surface area for EP was $S_{EP} \sim 12 \times 3$ mm$^2$, and as a result the constant current density was $J_{EP} = i_{EP}/2S_{EP} \sim 170$ mA/cm$^2$. During the process, hydrogen gas evolution could be observed at the cathode. The final Al surface looked mirror-like.

Since in our setup immersion of the beaker in the refrigerating bath was not compatible with stirring onto a magnetic plate, the temperature close by the Al anode was probably higher than $T_{bath}$ ($\sim$+10 °C difference has been measured in several cases). We tried to minimize this effect during anodization as compared to EP, by keeping the anode as close as possible to the external temperature controlled bath, using in this case a much smaller beaker (50 mL, filled up to 30 mL).

As the starting anodization EL, we chose an aqueous (DI water) solution of oxalic acid ($(COOH)_2$, Sigma-Aldrich, Italy), and decided to run this process as well as the EP at $T_{bath}$ =+7 °C without stirring. We have only run single anodization processes, and considered the inner APA surface (in contact with the Al substrate) as the test surface for the layer quality, that is the regular pore arrangement. The outer APA surface (in contact with the EL) has been checked as well, soon after anodization, for an estimation of the outer pore mouth diameter $d^{out}$.

The anodizations were all run in galvanostatic mode, changing as a parameter the anodization current $i$ and so the current density $J = i/2S_{anod}$, where $S_{anod}$ is the dipped anode surface. An $S_{anod} \sim 10 \times 3$ mm$^2$ was used, significantly smaller than $S_{EP}$, to be sure to anodize only electropolished Al surface, and to avoid that possible side effects occurring at the ambient air–EL meniscus insist on the same region during the two consecutive processing steps, (namely EP and anodization).

As ILs to test we chose two different commercially available room temperature (RT) water-soluble ILs, namely 1-butyl-3-methylimidazolium 2-(2-methoxyethoxy) ethyl sulfate ($C_{13}H_{26}N_2O_6S$, "IL1") and 1-butyl-3-methylimidazolium tetrafluoborate ($C_8H_{15}BF_4N_2$, "IL2"), both from Sigma-Aldrich. The choice was driven by the former being particularly rich in oxygen, possibly taking place in the anodization reaction in spite of the oxalic acid and/or water oxygen, and the latter being very easily soluble in water.

### Sample Characterization

The APA outer and inner surfaces were imaged by means of atomic force microscopy (AFM) with a MFP-3D instrument (Asylum Research, USA), operating in Tapping mode with gold-coated silicon cantilever probes NSG10 (NT-MDT, Russia). The probes had a nominal resonance frequency $\sim$250 kHz and standard tip (apex diameter $\sim$10 nm, aspect ratio $\sim$2.6). Apart from surface quality inspection, the AFM images of the outer APA surface have also been used for quantitative determination of the sample roughness by means of the root mean square (RMS) of the distribution of sample features height. The RMS values of at least three AFM images acquired in different regions with 10 μm scan size have been averaged for each APA sample.

The APA top surface wettability was measured with different solvents by means of sessile drop method, using a DataPhysics OCAH 200 at laboratory conditions (temperature 17–20 °C, relative humidity 40–60%). Droplets of

$\sim$1 μL volume (drop diameter $\sim$1 mm) have been used in all cases. Similarly to the RMS measurements, for the liquid contact angles (CAs), the values on at least three different regions on each sample have been averaged as well. For both used liquids and especially for the IL2 solution, the CAs were soon decreasing in time after touching the APA surface. The reported values have been measured immediately after contact ($t < 5$ s).

For removal of the Al substrate, which was necessary to determine the APA thickness $h$, we adopted a non-standard technique. The reason was that in our samples the Al was sandwiched between two adjacent APA films, and in these conditions, we found the standard dissolution in either saturated $HgCl_2$ [1, 4, 6, 34–38] or $CuCl_2$ [7, 8] not to be so effective as for one-side APA films on Al. Therefore, we decided to run a second EP-like process in much harder conditions than during the Al smoothing step, namely at RT and current density $\sim 10\ J_{EP}$. The hard Al etching was accompanied by a strong hydrogen bubbling at the cathode and by a typical noise, while quasi-periodic (1–2 Hz) Al spitting off between the two APA films was visible through the beaker walls. We stopped the process when we could see that a significant loss of Al had already occurred at the bottom of the dipped sample, sufficient for optical inspection (typically after a time $t \sim 30$ s). The APA thickness $h$ was then measured by optical micrographs acquired in reflection perpendicular to the film sections, with $a \pm 1$ μm resolution uncertainty.

## Results and Discussion

### Anodization in Bare Oxalic Acid

The preliminary EP step significantly improved the starting Al surface quality, as the local RMS roughness measured by AFM for 30 μm scan size changed from $\sim$150 nm to $\sim$5 nm. On this surface, APA was grown by anodization. According to the current understanding of the process [5, 14, 17], for a given EL the value of the electric field $E$ at the Al surface is the key parameter for optimal growth of APA. The process relies on the balance between the chemical dissolution rate of the pores and the diffusion rate of the ions involved in the chemical reactions of the anodization (namely the incoming $O^{2-}$ and the outcoming $Al^{3+}$, with respect to the anode). Since in first approximation of parallel plate electrodes at distance $g$, a uniform field between them applies $E = V/g$, where $V$ is the anodization voltage, potentiostatic anodization at constant $V$ seems to be the most appropriate mode for controlled growth of APA. However, the growth rate $v_g$ is actually correlated with the ion transport rate, and finally with the anodization current $i$. Therefore, galvanostatic anodization [39–41] is probably the most appropriate for controlling the final film thickness $h$, and this is the mode that we have adopted for our work. In Fig. 1a, a few voltage–time characteristic curves $V(t)$ acquired during galvanostatic anodization in our setup are displayed. The total anodization time was always set to $t_{end} = 30$ min, whereas the current density $J$ was varied. The oxalic acid concentration was 0.3 M, as reported in most works done with this EL [1, 3, 6, 11, 31, 34–36, 42–45].

Independent of the anodization mode, if either potentiostatic or galvanostatic, in the steady state both $i$ and $V$ should be constant over the process time $t$, as for ionic conduction it is $i \sim e^{\alpha V}$, with $\alpha$ an appropriate constant [5, 14]. However, $V(t)$ is linearly increasing in Fig. 1a after

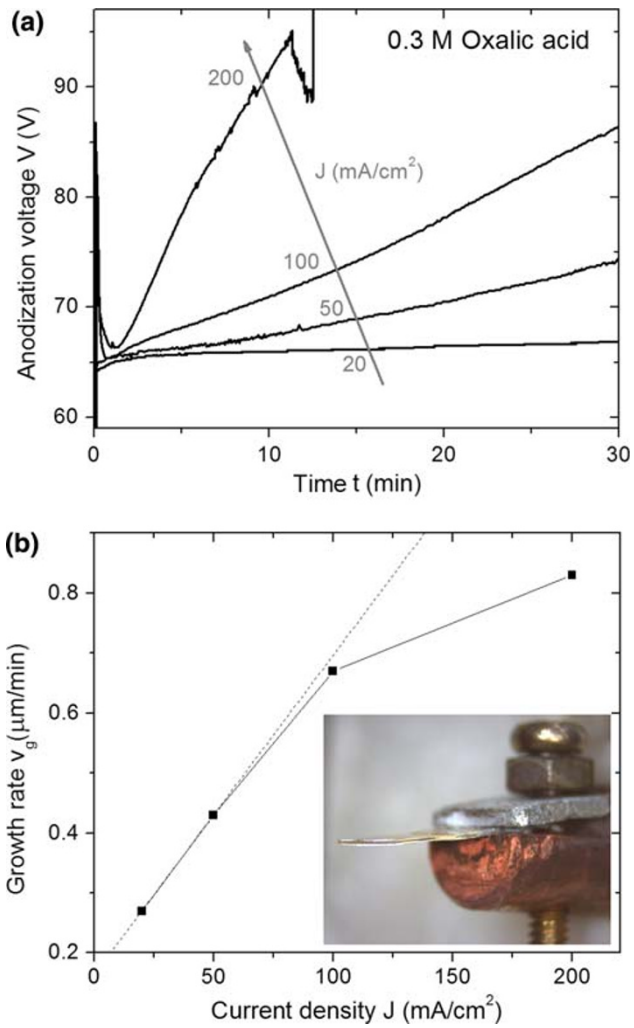


**Fig. 1** **a** $V(t)$ curves for anodization in bare oxalic acid (0.3 M) at different $J = 20$, 50, 100 and 200 mA/cm$^2$, from bottom to top curve. $T_{bath} = +7$ °C, no stirring, $t_{end} = 30$ min. **b** Final values of $h$ for the different $J$, as determined by optical microscopy after dissolution of the Al substrate. Inset: typical resulting double film APA

the initial transients, with different rates increasing in turn with $J$. This behavior shows that we were not in a condition of equilibrium for the different anodization reactions. The reason can be that in our setup immersion of the EL beaker in the cooling bath was not compatible with stirring onto a magnetic plate. Therefore, a local depletion of ions in the EL close to the anode, along with formation of a stable ion concentration gradient, can have occurred over time, which leads to a progressive increase in $V$ in order for the power supply to keep $J$ constant.

The $h$ values obtained at $t_{end} = 30$ min as a result of the corresponding anodizations have been plotted in Fig. 1b. If the same current efficiency of the process was maintained in all the anodizations and for all the process time period, a linear relationship between $J$ and $h$ was expected [5, 22]. However, after the initial increase in $h$ with increasing $J$ a tendency to saturation is observed in Fig. 1b. Obviously, a progressive reduction of the current efficiency has occurred, probably due to the appearance of side reactions different from the anodization ones [5].

Actually, side reactions can also occasionally lead to catastrophic events, such as shown in Fig. 1a for the curve at $J = 200$ mA/cm$^2$. In that case after reaching a critical value $V_{crit} \sim 95$ V in $t_{crit} \sim 12$ min, $V$ started to decrease with some fluctuations, and finally increased up to the maximum power supply voltage. The reason for the latter increase was that the Al foil was cut at the air–EL meniscus, and the piece of anode dipped in the EL fell on the bottom of the beaker, opening the circuit. The APA thickness measured for this sample was $h_{crit} = 11$ μm, such that the respective critical electric field was $E_{crit} = V_{crit}/h_{crit} \sim 8.6$ MV/m. This is ~36% lower than the dielectric strength of compact alumina, $E_{break} = 13.4$ MV/m [46]. Whereas this could be partly due to the porous nature of our alumina, we do not think that the origin of this behavior is the dielectric breakdown of the oxide due to the high $V$ reached. Instead, we assign the discontinuity in the curve to a temperature activated fast etching of the Al at the air–EL meniscus, where on fluctuations of the interface the bare Al can locally come into contact with the EL. In fact, when using a 10-fold diluted oxalic acid we could reach a $V_{crit} \sim 160$ V before that any similar catastrophic event occurred, with a respective $h_{crit} \sim 13$ μm, which gives $E_{crit} \sim 12.3$ MV/m, much closer to $E_{break}$. Furthermore, in the latter case, the final steep change of voltage was toward the zero (closed circuit with virtually no resistance), and there was no anode resection of the air–EL meniscus.

The limited improvement in $h$ obtained in the considered time period $t_{end}$ on increasing $J$ in bare oxalic acid resulted in a maximum (non-linear) mean growth rate $v_g^{max} = h_{crit}/t_{crit} \sim 0.83$ μm/min (obtained for $J = 200$ mA/cm$^2$).

In Fig. 2a, the results of a morphological analysis of the outer APA surface of the samples fabricated during the anodizations of Fig. 1 are displayed. By means of AFM, both the outer pore mouth diameter $d_{out}$ and the distance between adjacent pores $D_{out}$ have been measured [47], after averaging values extracted from cross-sections taken along differently oriented lines in the AFM images. The overall RMS surface roughness was also estimated.

All the quantities in Fig. 2a have been plotted versus the anodization current density $J$. One can see that $d_{out}$ is approximately constant within the errors, as expected, since it should depend only on the type of EL and on its concentration. The weak increase actually observed can be due to a local rise of the EL temperature and thus of the oxide dissolution rate, probably occurring during anodization. On the contrary, $D_{out}$ is clearly increasing with $J$. Indeed, $D_{out}$ should increase with $V$ [5, 14, 17], and our $V(t)$

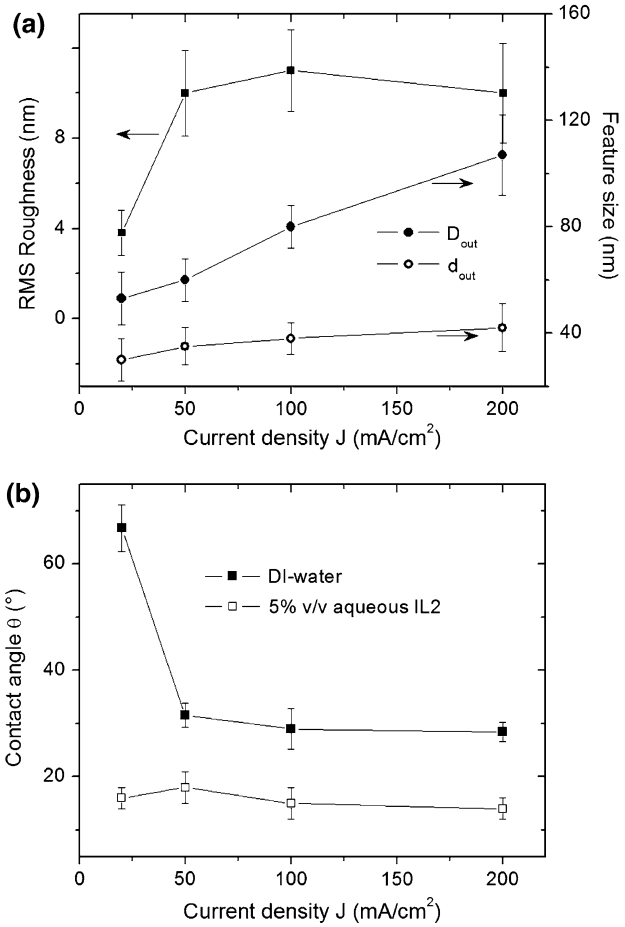


**Fig. 2** Morphological characterization of the outer surface of APA prepared in 0.3 M oxalic acid. **a** Results of the AFM measurements: pore diameter $d_{out}$ (*open circles*), interpore distance $D_{out}$ (*filled circles*), and surface RMS roughness values, for 10 μm scan size (*filled squares*). **b** Contact angles $\theta$ measured in ambient air on the same APA surfaces, using either DI water (*filled squares*) or a 10% v/v aqueous solution of IL2 (*open squares*), respectively

curves in Fig. 1a showed a $V$ that increased during each anodization. As a consequence, the roughness is almost constant for the higher $J$ values (i.e., the larger $D_{out}$), whereas it is significantly depressed for the lowest $J$ (i.e., the smallest $D_{out}$). We attribute this effect to the spatial "low-pass" characteristic of the AFM probe tip, which can hardly penetrate the smaller pores and thus senses the respective APA as an almost continuous, smooth surface.

## Anodizations in Oxalic Acid–IL Solutions

We then added our ILs to the oxalic acid starting solution. The amount of IL is expressed as the volume concentration c relative to the oxalic acid starting solution, (v/v, %). As we had little amount of ILs available (~4.2 mL for each type), we decided to work with a lower oxalic acid concentration, namely 0.03 M. In this way, we also planned to partially compensate for the expected increase in $i$ (for similar $V$) with respect to the bare oxalic acid EL due to the high electrical conductivity of the IL additive. In Fig. 3a, some $V(t)$ curves are displayed for anodizations, which were run in this diluted oxalic acid, all with $J \sim 100$ mA/cm$^2$. The effect of the 10-fold dilution of the acid can be seen in the dotted line (top most) curve of Fig. 3a, corresponding to an anodization run with external cooling ($T_{bath}$ =+7 °C) and without EL stirring. For the same $J$ as in Fig. 1a, an approximately two-fold increase in $V$ is observed. However, the final APA thickness was approximately the same ($h \sim 20$ μm grown in $t_{end} =$ 30 min), as expected in galvanostatic control, under the hypothesis of no decrease in current efficiency.

The general effect of addition of an IL in the EL, as compared to all the possible different anodization conditions for our setup, can also be seen in Fig. 3a. With respect to the dotted line curve, obtained for anodization run with external cooling and without stirring, the dashed line curve beneath it was obtained in the same EL also without stirring yet at RT. This curve presents a quite constant $V$ level (after the initial transients). Obviously the higher EL temperature allowed for maintaining a higher ionic mobility as well, and no local ion depletion at the anode occurred, different from the cooled EL condition, (Figs. 1a, 2a dotted line). A similar effect of approximately constant $V$ was observed when the anodization was run at RT and stirring was also activated, as shown by the continuous line curve beneath the dashed one. In this case, the $V$ level was even lower, as probably ion exchange and transport was further eased by the mechanical agitation, which was added to the thermal one. As a drawback obviously some instabilities were generated in the system, which resulted in strong fluctuations of $V$. The situation of both cooled and stirred 0.03 M oxalic acid EL is not shown, as it was not experimentally accessible in our setup,

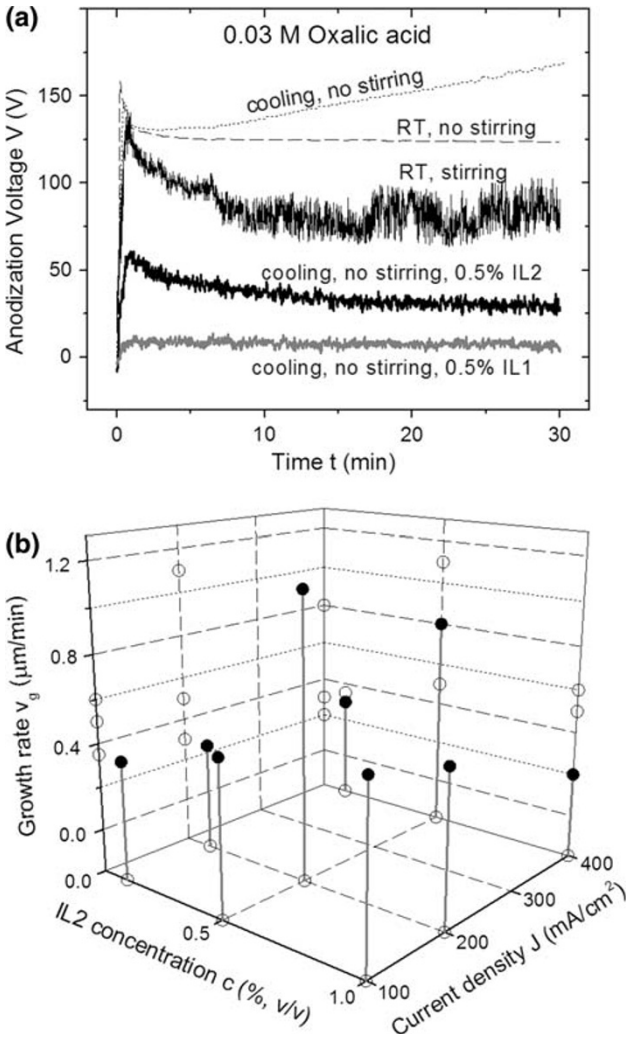


**Fig. 3** **a** $V(t)$ characteristic curves obtained for galvanostatic anodization ($J = 100$ mA/cm$^2$) in 0.03 M oxalic acid for $t_{end} = 30$ min under different conditions. From top to bottom: *dotted line*: same conditions as in Fig. 1a (i.e., with cooling and without stirring) but the 10-fold diluted EL. *Dashed line*: RT, no stirring. *Continuous line*: RT, stirring. *Thick line*: cooling, no stirring, IL2 additive with $c = 0.5\%$ v/v. *Thick gray line*: cooling, no stirring, IL1 additive with c = 0.5% v/v. **b** Values of $v_g$ measured for $t_{end} = 30$ min, for different combinations of IL2 relative concentration $c$ and current density $J$. (*Void circles*: projections of the data points to the axis planes)

but we would also expect a similar situation of approximately constant $V(t)$, with intermediate $V$ level lying between the high (RT, stirring) and the low (cooling, no stirring) ion mobility conditions. The $V(t)$ curves for anodization with cooled EL and no stirring (i.e., low ion mobility condition) but with IL content $c = 0.5\%$ are also reported in Fig. 3a (thick black line for IL2 and thick gray line for IL1, respectively). One can see that the $V$ level at regime was constant also in the latter cases, but significantly lower than for all the no-IL containing EL conditions. This was obviously due to the increased electrical conductivity of the EL after injection of the IL ions.

From Fig. 3a, it is clear that by keeping $V$ low via the IL additive one can run anodization at comparatively high $i$ as compared to standard values reported in the literature for bare oxalic acid EL, and still operate in MA condition. This should allow for avoiding detrimental effects such as the barrier breakdown observed in Fig. 1a. Furthermore, in case of two-step anodization it would help to keep the conditions as close as possible to the $V$ desired for optimal ordered APA growth, which for potentiostatic process in oxalic acid is in the 40–60 V range [5, 10, 17].

The resulting conductivity of the IL1-added EL was four times as much for the IL2-added EL. This could make one think that the performance of IL1 solutions in APA growth would be better. However, APA films were observed after anodizations run with IL1 solutions only for the lowest relative concentration values explored, namely $c = 0.01\%$, and with comparatively low $J = 20$ mA/cm$^2$. In those conditions, $h$ was quite low, as expected ($h_{IL1} = 5$–10 μm). For higher $J$ and/or higher $c$, no APA film was obtained at all, and on the contrary black pits were always observed on the Al substrate. At $c = 0.5\%$ and $J = 600$ mA/cm$^2$, in particular, anodization resulted in complete dissolution of the anode during successive rinsing in DI-water. Obviously the result of the high oxygen content, associated with the quite high conductivity (i.e., ion mobility), makes the dominating effect of IL1 to be a heavy ion bombardment of Al, rather than a support to the flow of the EL ions.

For the IL that on the contrary demonstrated to provide APA after most preliminary test anodizations, namely IL2, we decided to systematically investigate the results of the processes run for different combinations of $c$ and $J$ parameters, in the range $c = 0.01$–$2\%$ and $J = 20$–600 mA/cm$^2$. In particular, in Fig. 3b, a part of the ($c$, $J$) "phase" space for all the combinations of the values $c = 0.1\%$, $0.5\%$, and $1.0\%$ and $J = 100$, 200, and 400 mA/cm$^2$ is shown, with respect to the resulting APA growth rate. It turns out that a local maximum of $v_g$ was found for the point ($c$, $J$) = (0.5%, 200 mA/cm$^2$), with value $v_g^{max}$ (IL2) = 1.1 μm/min. This growth rate is higher than for the same acidic EL with 10-fold higher concentration (see Fig. 1b) and more than three times higher than for the EL solution with the same acid concentration ($V(t)$ dotted line curve in Fig. 3a, $v_g \sim 0.3$ /min).

Obviously, some improvement due to IL2 ions occurs only at intermediate $c$ and $J$ values. For $J$, side effects can be imagined to negatively affect APA formation on excessive increase of this parameter, such as an extraordinary local EL heating, with a consequent loss of current efficiency. On the other hand, too many IL ions in solution can overwhelm the other EL ions, and decrease the current efficiency in turn. We can work out the molar ratio of the IL–oxalic acid species in the experimentally observed best condition of 0.5% v/v for IL2. The numbers of moles for each species can be calculated as $n_{ox} = M_{ox}V_{ox}$, where $M_{ox}$ is the molarity and $V_{ox}$ the volume of oxalic acid, and $n_{IL2} = m_{IL2}/MW_{IL2}$, where $m_{IL2}$ is the mass and $MW_{IL2}$ the molecular weight of IL2, respectively. Therefore, the molar ratio is $n_{ox}/n_{IL2} = M_{ox}MW_{IL2}/\rho_{IL2}c$, with $\rho_{IL2}$ the mass density of IL2. Since it is $MW_{IL2} = 226.03$ g/mole and $\rho_{IL2} = 1.21$ g/mL, for $c = 0.5\%$ it turns out $n_{ox}/n_{IL2} \sim 1.1$. Therefore, the best improvement in $v_g$ on addition of IL2 is obtained for $a \sim 1{:}1$ ratio of the IL2 moles with respect to the moles of the oxalic acid. When this ratio was increased of a factor two, it was not possible to grow APA any more even with IL2. On the contrary, anodization run with the same ratio, obtained for example by doubling both concentrations ($M_{ox} = 0.06$ M and $c_{IL2} = 1\%$), produced APA with consistent $h$ values. The color of the respective outer APA surfaces was also quite similar, pale yellow in all cases, as usually observed due to inclusion of oxalate ions [5, 14].

The molar ratio for the same relative concentration $c = 0.5\%$ in the case of the other IL can also be calculated. For IL1, being $MW_{IL1} = 338.42$ g/mole and $\rho_{IL1} = 1.19$ g/mL, it turns out $n_{ox}/n_{IL1} \sim 1.7$. This value is of the same order of magnitude as for IL2. Anyway even for $c = 0.1\%$, no APA was obtained in the case of IL1, such that this negative result can only be assigned to an inherent chemical difference between the interaction of the two ILs with the oxalic acid.

## IL Aided Characterization and Processing

After using the IL2 as an additive in anodization, we have also tried to take advantage of its properties in the characterization of the system. In Fig. 2b, the liquid CAs $\theta$ measured on the APA surfaces described in Figs. 1, 2a have been reported. The filled squares represent the CAs obtained with DI-water as the wetting phase. One can see that all the respective APA films look rather hydrophilic ($\theta_{water} < 90°$). Most samples showed quite similar values ($\theta_{water} \sim 29°$), whereas only the sample with smaller pores showed a significantly higher $\theta_{water}$. The reason is probably that for that sample the pores were too small to be filled by the water, and the drop was actually sitting on a mixed APA–air interface [48]. In practical terms, the water "probe" did not allow for high enough resolution to sense the smallest APA pores. A similar resolution limit affected also the topographic measurements by AFM, as observed in the RMS roughness plot of Fig. 2a (see the previous subsection for discussion). In Fig. 2b, the open squares report instead the CAs obtained with a $c = 10\%$ v/v solution of IL2 in the DI-water wetting phase, $\theta_{IL2}$. In this case, the CA values were all quite similar to each other, and lower than for the bare water, $\theta_{IL2} \sim 16°$. This means

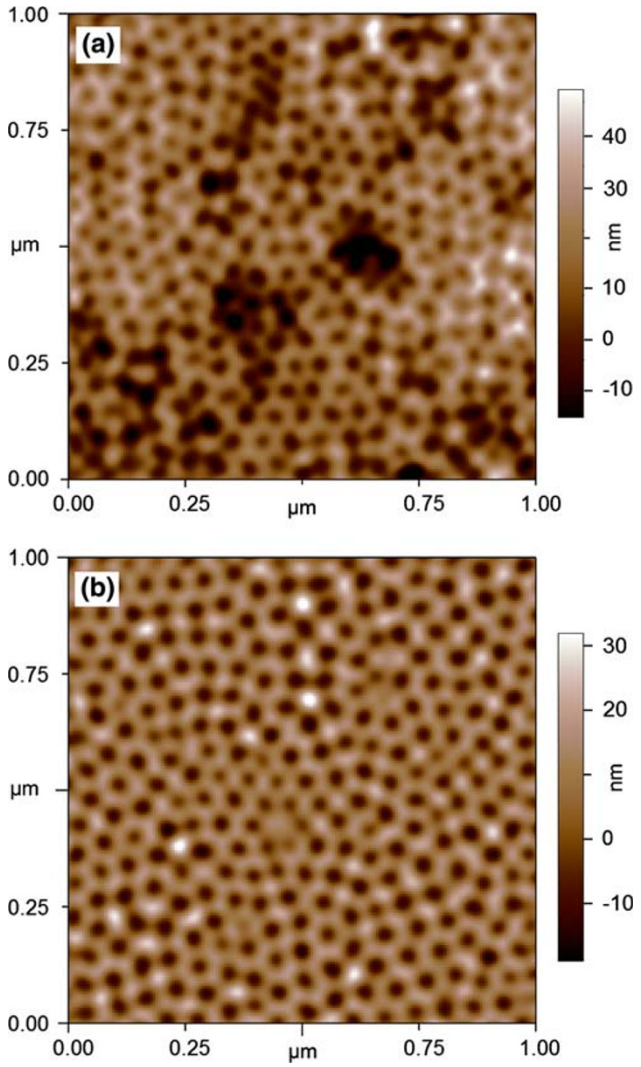


**Fig. 4** Typical APA inner surface, in which the closed pore bottoms have been partly opened by immersion in 1 M oxalic acid at 30 °C for 30 min, in the following conditions: **a** APA after cleaning only and **b** APA after cleaning and keeping in 10% IL2 aqueous solution for 10 min. Both images have been smoothed with a 3x3 kernel Gaussian filter

that the IL2 solution had higher wetting power than water, and could wet even the smallest APA pores. Actually a similar behavior is expected from any IL, which should work such as a highly polar solvent that can easily penetrate voids of a few nanometer diameter only [3]. Therefore, IL2 can also be used successfully for this kind of characterization of the porous APA surface morphology.

We then decided to test the above property of IL2 in a further processing step of our APA surfaces, namely the pore opening. We performed this operation in concentrated, warm oxalic acid (1 M, $T_{bath}$ =+30 °C) for 30 min. Before that, for some APA samples, the surface was simply rinsed in DI-water and blown dry with $N_2$ (for $t > 30$ s). For some other APA samples, the cleaned surface was also submerged in IL2 diluted aqueous solution for 10 min. Two representative AFM images of inner APA surface after pore opening without and with IL2 solution wet pores can be seen in Fig. 4a, b, respectively. Similar results have been obtained in several regions of different APA samples. Both images in Fig. 4 refer to an early stage of etching, for which only some pore bottoms have already been removed, and the exposed surface is still comparatively close to the originally exposed one (depth < 100 nm). Obviously exposure of APA to the IL2-water solution provided some level of protection of the pore sidewalls after pore bottom opening. The reason is that the inner pore voids cannot be easily penetrated by the etching solution, after capillary effect, as they are already occupied by the IL2-water solution instead. We have estimated that for the considered etching stage about 20% of the imaged areas were still covered by pores that were not yet opened, in both cases of samples exposed or not to IL2–water solution, whereas the laterally over-etched areas changed from ~25% to ~5% in the case of IL2–water wet APA.

## Conclusions

The effect of addition of ILs into an oxalic acid aqueous solution commonly used for the fabrication of APA has been investigated. Two different ILs have been used for the first time as additives in this anodization process. By adding one of them, namely 1-butyl-3-methylimidazolium tetrafluoborate, in an approximately 1:1 molar ratio with the solution acid, and properly tuning the current density, we could obtain a growth rate of APA of 1.1 μm/min. This growth rate is comparable to the value normally obtained in the industrially applied HA conditions, but has been obtained in MA conditions in our case. Therefore, our process should make it possible to obtain thick APA layers in comparatively short times (order of few hours) and with ordered pore arrays also on the outer surface, after two-step anodization in the appropriate $V$ range. The high-anodization current in itself does not guarantee fast APA growth, as demonstrated when the other IL was used as the EL additive. Therefore, a better understanding of the chemical mechanisms underlying the observed increase in growth rate has to be pursued, and is currently the subject of further research activity in our group. However, the presently reported preliminary results hold promise for the development of a technologically viable procedure for the fast growth of APA. In this application perspective, the possible use of ILs in characterization of the porous film and in its subsequent processing has also been explored. As a result, the selected IL has been demonstrated to be useful also as a pore wall protection medium during pore opening of APA, a process step that is often taken when passing membranes are fabricated out of the supported porous surfaces.

**Acknowledgments** The authors would like to thank Mr. Romeo Losso for providing the original idea of using ionic liquids in the preparation of anodic porous alumina and for the recommendations, thereafter, and Mr. Claudio Larosa for technical support and useful discussions on the topic.

## References

1. H. Masuda, K. Fukuda, Science **268**, 1466 (1995). doi:10.1126/science.268.5216.1466
2. S. Ono, M. Saito, H. Asoh, Electrochim. Acta **51**, 827 (2005). doi:10.1016/j.electacta.2005.05.058
3. R. Redon, A. Vazquez-Olmos, M.E. Mata-Zamora, A. Ordonez-Medrano, F. Rivera-Torres, J.M. Saniger, Rev. Adv. Mater. Sci. **11**, 79 (2006)
4. E. Stura, D. Bruzzese, F. Valerio, V. Grasso, P. Perlo, C. Nicolini, Biosens. Bioel. **23**, 655 (2007). doi:10.1016/j.bios.2007.07.011
5. G.E. Thompson, Thin Solid Films **297**, 192 (1997). doi:10.1016/S0040-6090(96)09440-0
6. C.L. Liao, C.W. Chu, K.Z. Fung, I.C. Leu, J. Alloy Compd. **441**, L1 (2007). doi:10.1016/j.jallcom.2006.09.084
7. Y. Li, Z.Y. Ling, S.S. Chen, J.C. Wang, Nanotechnology **19**, 225604 (2008). doi:10.1088/0957-4484/19/22/225604
8. W. Chen, J.-S. Wu, X.-H. Xia, ACS Nano **2**, 959 (2008)
9. P. Yang, M. An, C. Su, F. Wang, Electrochim. Acta **54**, 763 (2008). doi:10.1016/j.electacta.2008.06.064
10. Y.C. Sui, J.M. Saniger, Mater. Lett. **48**, 127 (2001). doi:10.1016/S0167-577X(00)00292-5
11. J.-H. Zhou, J.-P. He, G.-W. Zhao, C.-X. Zhang, J.-S. Zhao, H.-P. Hu, Trans. Nonferrous Met. Soc. China **17**, 82 (2007). doi:10.1016/S1003-6326(07)60052-1
12. N. Tsuya, T. Tokushima, M. Shiraki, Y. Wakui, Y. Saito, H. Nakamura, S. Hayano, A. Furugori, M. Tanaka, IEEE Trans. Magn. **22**, 1140 (1986). doi:10.1109/TMAG.1986.1064316
13. X. Bao, F. Li, R.M. Metzger, J. Appl. Phys. **79**, 4866 (1996). doi:10.1063/1.361635
14. J.W. Diggle, T.C. Downie, C.W. Goulding, Chem. Rev. **69**, 365 (1969). doi:10.1021/cr60259a005
15. C.R. Martin, Chem. Mater. **8**, 1739 (1996). doi:10.1021/cm960166s
16. M. Lohrengel, Mater. Sci. Eng. Rep. **11**, 243 (1993). doi:10.1016/0927-796X(93)90005-N
17. F. Li, L. Zhang, R.M. Metzger, Chem. Mater. **10**, 2470 (1998). doi:10.1021/cm980163a
18. M. Nakao, S. Oku, T. Tamamura, K. Yasui, H. Masuda, Jpn J. Appl. Phys. **38**, 1052 (1999). doi:10.1143/JJAP.38.1052
19. A.-P. Li, F. Müller, A. Birner, K. Nielsch, U. Gösele, Adv. Mater. **11**, 483 (1999). doi:10.1002/(SICI)1521-4095(199904)11:6<483::AID-ADMA483>3.0.CO;2-I
20. F. Müller, A. Birner, J. Schilling, A.P. Li, K. Nielsch, U. Gösele, V. Lehmann, Microsyst. Technol. **8**, 7 (2002). doi:10.1007/s00542-002-0047-3
21. G. Sauer, G. Brehm, S. Schneider, K. Nielsch, R.B. Wehrspohn, J. Choi, H. Hofmeister, U. Gösele, J. Appl. Phys. **91**, 3243 (2002). doi:10.1063/1.1435830
22. P. Bocchetta, C. Sunseri, G. Chiavarotti, F. Di Quarto, Electrochim. Acta **48**, 3175 (2003). doi:10.1016/S0013-4686(03)00348-7
23. A. Mozalev, S. Magaino, H. Imai, Electrochim. Acta **46**, 2825 (2001). doi:10.1016/S0013-4686(01)00497-2
24. Anopore™ Inorganic Aluminum Oxide Membrane Filters, http://www.2spi.com/catalog/spec_prep/filter2.shtml, SPI Supplies & Structure Probe, Inc., 569 East Gay Street, West Chester, PA 19380, USA
25. F. Li, R.M. Metzger, J. Appl. Phys. **81**, 3806 (1997). doi:10.1063/1.364776
26. M. Sun, G. Zangari, R.M. Metzger, IEEE Trans. Magn. **36**, 3005 (2000). doi:10.1109/20.908488
27. H.J. Fan, W. Lee, R. Scholz, A. Dadgar, A. Krost, K. Nielsch, M. Zacharias, Nanotechnology **16**, 913 (2005). doi:10.1088/0957-4484/16/6/048
28. S. Grimm, R. Giesa, K. Sklarek, A. Langner, U. Gösele, H.-W. Schmidt, M. Steinhart, Nano Lett. **8**, 1954 (2008). doi:10.1021/nl080842c
29. J. Liang, H. Chik, A. Yin, J. Xu, J. Appl. Phys. **91**, 2544 (2002). doi:10.1063/1.1433173
30. R.B. Wehrspohn, A. Birner, F. Müller, J. Nielsch Schilling, U. Gösele, *Pits and Pores* (Electro-chemical Society Proceedings, Pennington, 2000)
31. W. Lee, R. Ji, U. Gösele, K. Nielsch, Nat. Mater. **5**, 741 (2006). doi:10.1038/nmat1717
32. P. Wasserscheid, T. Welton, *Ionic Liquids in Synthesis* (Wiley-VCH Verlag GmbH & Co. KGaA, Weinheim, 2007)
33. B. Weyershausen, K. Lehmann, Green Chem. **7**, 15 (2005). doi:10.1039/b411357h
34. T. Xu, G. Zangari, R.M. Metzger, Nano Lett. **2**, 37 (2002). doi:10.1021/nl010075g
35. H. Masuda, H. Yamada, M. Satoh, H. Asoh, M. Nakao, T. Tamamura, Appl. Phys. Lett. **71**, 2770 (1997). doi:10.1063/1.120128
36. A.P. Li, F. Müller, A. Birner, K. Nielsch, U. Gösele, J. Appl. Phys. **84**, 6023 (1998). doi:10.1063/1.368911
37. H. Masuda, K. Yada, A. Osaka, Jpn J. Appl. Phys. **37**, L1340 (1998). doi:10.1143/JJAP.37.L1340
38. A.P. Li, F. Müller, A. Birner, K. Nielsch, U. Gösele, J. Vac. Sci. Technol. A **17**, 1428 (1999). doi:10.1116/1.581832
39. A. Zahariev, I. Kanazirski, A. Girginov, Inorg. Chim. Acta **361**, 1789 (2008). doi:10.1016/j.ica.2007.03.040
40. W. Lee, R. Scholz, U. Gösele, Nano Lett. **8**, 2155 (2008). doi:10.1021/nl080280x
41. N. Bwana, J. Nanopart. Res. **10**, 313 (2008). doi:10.1007/s11051-007-9253-3
42. M.H. Rahimi, S.H. Tabaian, S.P.H. Marashi, M. Amiri, M.M. Dalaly, S. Saramad, A. Ramazani, A. Zolfaghari, Int. J. Mod. Phys. B **22**, 3267 (2008). doi:10.1142/S0217979208048206
43. L. Zhang, H.S. Cho, F. Li, R.M. Metzger, W.D. Doyle, J. Mater. Sci. Lett. **17**, 291 (1998). doi:10.1023/A:1006577504924
44. W. Lee, K. Schwirn, M. Steinhart, E. Pippel, R. Scholz, U. Gösele, Nat. Nano **3**, 234 (2008). doi:10.1038/nnano.2008.54
45. K. Nielsch, F. Müller, A.P. Li, U. Gösele, Adv. Mater. **12**, 582 (2000). doi:10.1002/(SICI)1521-4095(200004)12:8<582::AID-ADMA582>3.0.CO;2-3
46. W. Martienssen, H. Warlimont, *Springer Handbook of Condensed Matter and Materials Data* (Springer, Berlin, 2005)
47. S. Shingubara, J. Nanopart. Res. **5**, 17 (2003). doi:10.1023/A:1024479827507
48. A.B.D. Cassie, S. Baxter, Trans. Faraday Soc. **40**, 546 (1944). doi:10.1039/tf9444000546